Int. J. Electrochem. Sci., 7 **(2012)** 8745 - 8752

International Journal of
ELECTROCHEMICAL
SCIENCE
www.electrochemsci.org

Short Communication

A SiO/graphene Nanocomposite as a High Stability Anode Material for Lithium-Ion Batteries

Chenfeng Guo, Dianlong Wang[*]*, Qiuming Wang, Bo Wang, Tiefeng Liu*

School of Chemical Engineering and Technology, Harbin Institute of Technology, Heilongjiang 150001, PR China
[*]E-mail: wangdianlonghit@163.com

Received: 24 July 2012 / *Accepted:* 13 August 2012 / *Published:* 1 September 2012

A novel anode material for lithium-ion batteries, SiO/graphene nanocomposite, was fabricated by a facile *in situ* chemical synthesis approach. The nanocomposite were characterized by X-ray diffraction, field emission scanning electron microscopy and high resolution transmission electron microscopy. SiO nanoparticles with sizes of about 50-300 nm were homogeneously located on graphene matrix. The prepared nanocomposite material exhibits an high initial specific capacity of 2285 mAh g^{-1}, excellent cyclic performance of 890 mAh g^{-1} at 100th cycle and good rate capability, which was ascribed to the three-dimensional architecture of SiO/graphene nanocomposite. Our results indicate that SiO/graphene nanocomposite is a good candidate for high performance lithium-ion battery anodes.

Keywords: Silicon monoxide; Graphene; Nanocomposite; Anode; Lithium-ion batterys

1. INTRODUCTION

Nowadays, to meet requirements for various ranges of applications, including portable electronics, high power hybrid vehicles or electric vehicles, rechargeable solid-state batteries, such as lithium-ion batteries (LIBs) should be endowed with higher energy and power densities, lower cost, higher cycling life [1]. A lot of attention has been focused on finding alternative anode materials, which could show higher gravimetric and volumetric capacities than commercialized graphite (LiC_6:372 mAh g^{-1}) [2]. Silicon monoxide (SiO)-based materials have long been considered as anode materials for LIBs because of their high capacities [3-6]. However, the SiO anode materials have poor cycle performance because of agglomerations and huge volume change of active materials during lithium insertion/extraction process. In order to overcome the volume mismatch and improve the cycle performance, many strategies have been reported, such as employing small SiO particles (reducing the

particle size) in carbonaceous matrixes [3,4,5,7], improving the electrochemical performance by changing to more effect binders [8], enhancing the initial coulombic efficiency by using a lithium pre-doping method [9] or a SiO/lithium double layer anode [10].

Graphene is an excellent matrix on which to anchor LIBs active materials due to its superior electrical conductivity [11], excellent mechanical flexibility and good chemical stability [12]. Although many graphene-based materials (SnO_2, Fe_2O_3, Fe_3O_4, NiO, CeO_2, Co_3O_4, CuO/graphene) [13-19] as anode materials for LIBs have been reported, to the best of our knowledge, there were fewer reports on the SiO/graphene nanocomposite as an anode material for LIBs so far. Herein, we report a facile *in situ* chemical synthesis method for preparing SiO/graphene nanocomposite. Electrochemical tests indicate that the SiO/graphene nanocomposite exhibits high specific capacity, excellent rate capability and cycling stability as anode material for LIBs.

2. EXPERIMENTAL SECTION

2.1 Preparation of sample

The SiO/graphene nanocomposite was prepared by an *in situ* chemical synthesis method using graphite oxide (GO) and SiO nanopaticles as the precursor. GO was prepared according to modified Hummers method [20].To obtain SiO nanopaticles, commercially available SiO powders (Aldrich) with an average particle size of 40 μm were milled in high efficient attritor mill (Union Process, type 01-HD/HDDM) with intensive rotation speed at 2000 rpm for 2 h. To prepare the composite material, 100 mg SiO nanopaticles were added into 100 ml (1mg ml^{-1}) of GO dispersion, followed by 2h ultrasonication. The mixed aqueous suspension of the GO and SiO nanopaticles was then reduced with 4000μl of NH_4OH and 250μl of hydrazine (NH_2NH_2, 35 wt.%) at 100 °C, with continuous stirring for 4h. The resultant solid products were collected by filtration and dried in vacuum at 80 °C for 12 h. To remove the residual water molecules and functionals in the graphene sheets, the product was annealed at 500 °C for 1h in Ar atmosphere. For comparison, bare graphene were synthesized by the same method.

2.2 Materials Characterization

Powder X-ray diffraction (XRD) analyses were performed on Rigaku D/MAX-RC X-ray diffractometer with Cu Ka 1 (45 kV and 50 mA). Raman spectrum was acquired on a Jobin Yvon HR800 confocal Raman system with 632.81nm diode laser excitation. Thermogravimetric (TGA) analysis was performed on a Netzsch STA449C system. Field emission scanning electron microscope (FESEM) analysis was performed on a Hitachi S-4700 equipped with energy dispersive X-ray analysis (EDAX). Transmission electron microscopy (TEM) and high resolution TEM (HRTEM) analyses were performed on a JEM-2100F microscope with an accelerating voltage at 200kV.

2.3 Electrochemical measurements

Electrochemical properties of the products were measured using CR2025 coin cells. Electrodes were prepared by casting the slurry consisting of 80% active material, 10% sodium carboxymethyl cellulose (CMC), and 10% acetylene black onto a copper foil. The fabrication process of cells can be found elsewhere [21]. The cells were galvanostatically charged and discharged under different current densities over a voltage range of 0.01-2.5V on a Neware battery tester.

3. RESULTS AND DISCUSSIONS

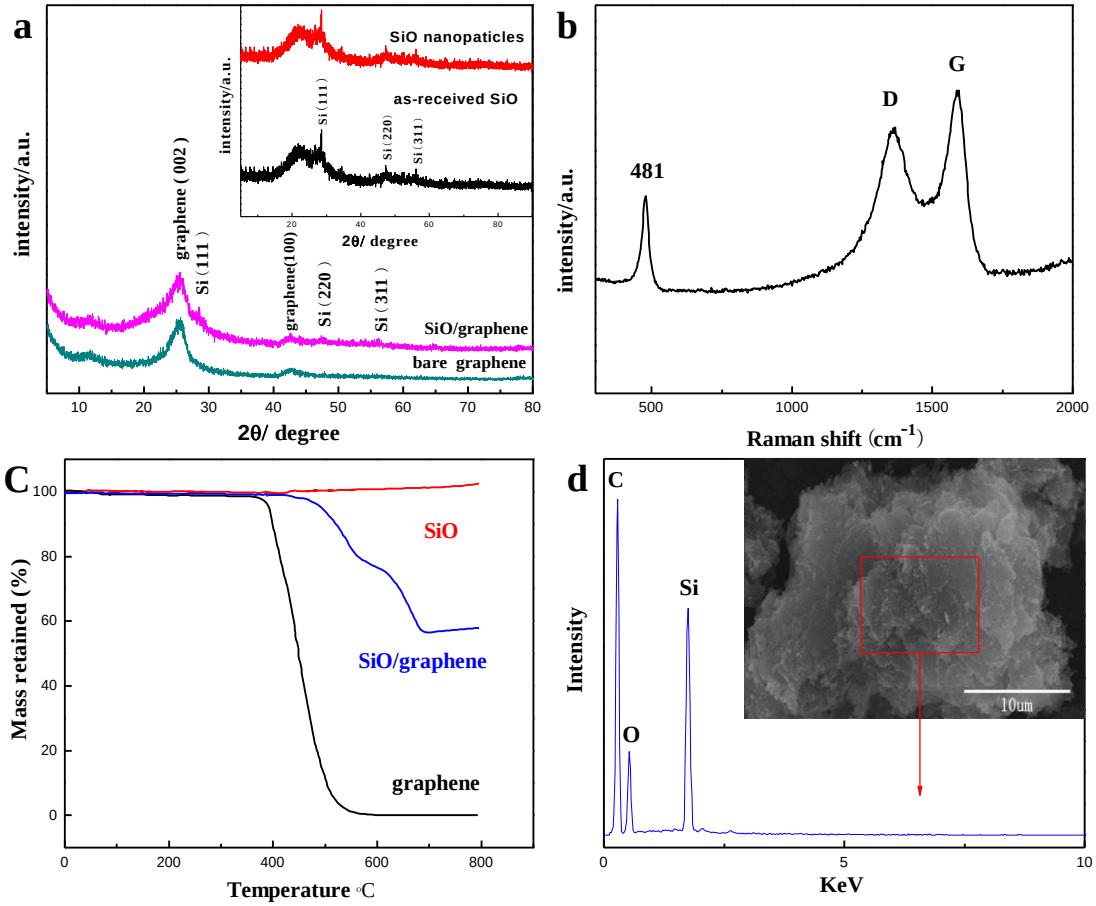

Figure 1.(a) XRD patterns of bare graphene and SiO/graphene nanocomposite, inset of (a): XRD patterns of as-received SiO and SiO nanopaticles. (b) Raman spectra of SiO/graphene nanocomposite. (c) TGA curves of SiO nanopaticles, SiO/graphene and bare graphene. (d) EDAX spectra from the surface of SiO/graphene nanocomposite.

The XRD patterns obtained from the samples are shown in Figure 1a. From both the patterns of as-received SiO and SiO nanopaticles, there is a broad peak located at 23°, which indicates the amorphous nature of the powders. The weak peaks of 28.4°, 47.3° and 56.1° are consistent with the standard values of Si (JCPDS no.27-1402), suggesting that amorphous SiO contains dispersed Si

crystal phases [22,23]. The attritor-milling had no significant effect on the XRD patterns except a slight decrease of the Si peak. Both bare graphene and the SiO/graphene nanocomposite show a strong (002) diffraction peak around 26° and a weak (100) diffraction peak at 42.8°. All the positions of diffraction peaks of SiO/graphene nanocomposite are in good agreement with SiO and graphene, there are no new peaks coincident with other impurities. Figure 1b is the Raman spectrum of SiO/graphene nanocomposite. As can be seen in Figure 1b, the peaks detected at 1355 and 1604 cm^{-1} are located near to the typical D and G peaks of graphene [24]. The large band at around 481 cm^{-1} can be assigned to SiO nanoparticles [25]. According to the TGA shown in Figure 1c, the composition of SiO in the SiO/graphene nanocomposite was 57 wt.%. These evidences indicate that the SiO/graphene nanocomposite was successfully prepared via the *in situ* chemical synthesis method from GO and SiO nanoparticles.

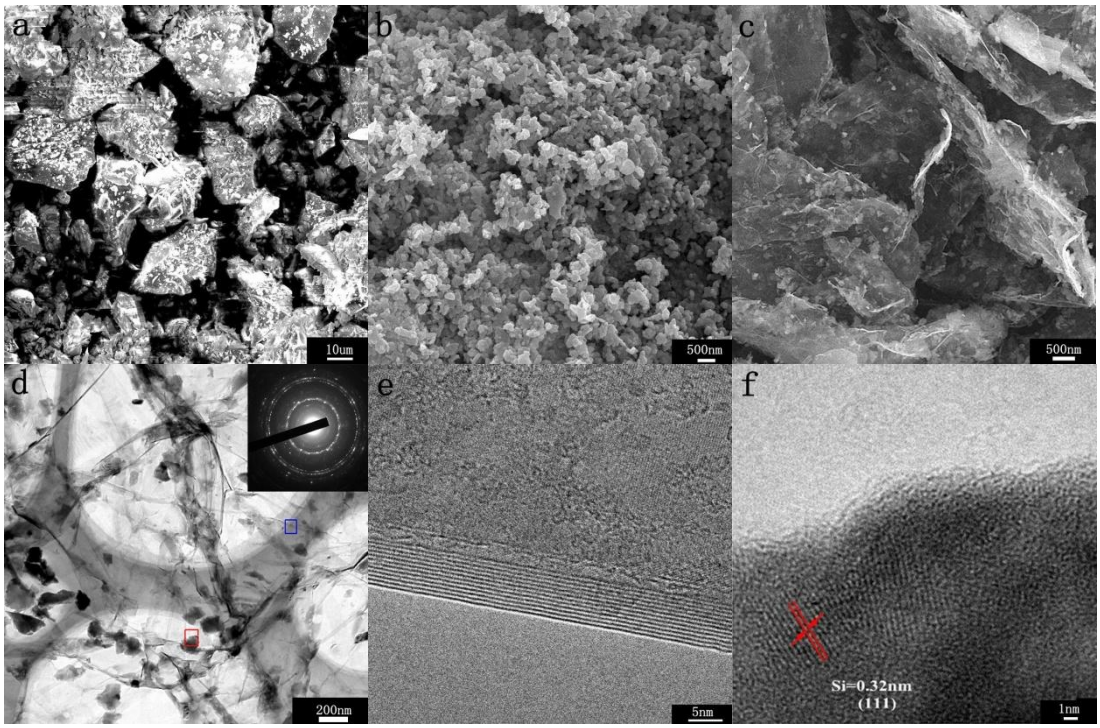

Figure 2.(a) FESEM image of as-received SiO powder. (b) FESEM image of SiO nanopaticles. (c) FESEM image of SiO/graphene nanocomposite. (d) TEM image of SiO/graphene nanocomposite, inset of (d): SAED of Si domain in SiO nanopaticles. (e) HRTEM image of graphene in the SiO/graphene nanocomposite (the blue rectangle region in (d)). (f) HRTEM image of SiO/graphene nanocomposite (the red rectangle region in (d)).

The FESEM images of as-received SiO powder and SiO nanopaticles are presented in Figure 2a and b in order to compare their morphologies. The initial particle size of 40 μm was reduced to 50-300 nm by attritor-milling. From the FESEM image of SiO/graphene nanocomposite (Figure 2c), SiO nanoparticles are uniformly and densely distributed on the surfaces of graphene. We also observed the insertion of SiO nanoparticles between the interlayers of the graphene and the nanoporous composite with large amount of cavities was formed. The TEM image of the nanocomposite (Figure 2d) reveals a

morphology feature which is in agreement with the FESEM result, graphene act as supporting materials for anchoring of SiO nanoparticles. The SAED pattern (the inset image in Figure 2d) comprises a well-resolved set of concentric rings with bright spots, indicating the nanocrystalline nature of the Si domain in SiO microstructure. Figure 2e was recorded from the blue rectangle region in Figure 2d. The distinguishable lines in parallel in Figure 2e correspond to the fold of graphene. It is found that the graphene platelet thickness ranged from 4 to 5 nm, which corresponds to an approximately 12-15 layers stacking of the monoatomic graphene. Figure 2f displays the HRTEM image of the red rectangle region in Figure 2d. Lattice fringes were clearly displayed, and the d-spacing of this SiO nanoparticles was derived to be 0.32 nm, corresponding to the spacing between (111) planes of nanocrystalline Si. EDAX analysis were used on SiO/graphene nanocomposite to quantify the atomic composition of the sample. The EDAX spectra (Figure 1d) shows that the elements present include Si, O and C on the surface of as-synthetized composite and verifies the existence of Si and O with approximately 1:1 ratio implying its stoichiometry, SiO.

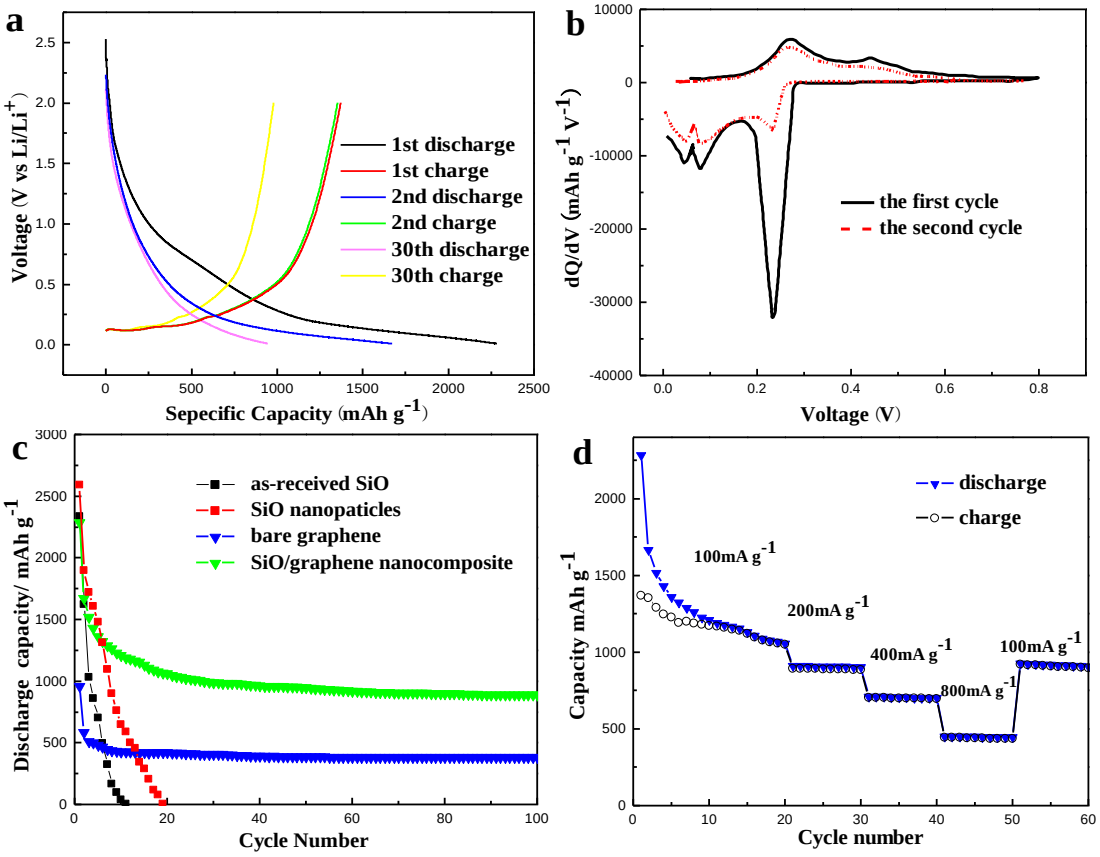

Figure 3.(a) Charge/discharge profiles of SiO/graphene in the 1st, 2nd and 30th cycle. (b) Differential capacity curves of SiO/graphene electrode. (c) Cycling performance of as-received SiO, SiO nanoparticles, bare graphene and SiO/graphene nanocomposite as anode materials at a current of 100 mA g^{-1}. (d) Cycling performance of SiO/graphene electrode at various current densities.

Figure 3a shows the 1st, 2nd and 30th charge-discharge curves of SiO/graphene electrode at a current density of 100 mA g^{-1} in a voltage range of 0.01-2.5 V vs Li^+/Li. The initial small plateaus at

0.8 V and long slope profiles of SiO/graphene electrode is similar to bare SiO electrode that reported previously [5]. As for the electrochemical performance, the SiO/graphene electrode exhibits a discharge capacity of 2285 mAh g^{-1} and a coulombic efficiency of 60%, respectively. Large irreversible capacity observed in the first cycle may be attributed to the formation of solid electrolyte interface (SEI) and the reaction of lithium ion with oxygen containing functional groups [27]. Figure 3b is differential capacity curves (dQ/dV vs.voltage) of SiO/graphene electrode in the potential range of 0.01-2.5 V, showing the information about their structural transformations during lithiation and delithiation. In the first discharge process of SiO/graphene electrode, three peaks are observed at 0.24, 0.08 and 0.05 V. The peak at 0.24 V with reduced intensity reappeared during the second discharge, indicating that the reversible and irreversible reactions of SiO with lithium occurred simultaneously [22]. The peak at 0.08 V can be observed in the following discharge processes, corresponding to phase transitions between amorphous Li_xSi [26]. The peak at 0.05V is corresponding to the lithium insertion into graphene [16]. During the first and second lithium extraction, there are also two broad peaks corresponding to reversible reaction at 0.28 and 0.45 V. Figure 3c shows the curves of discharge capacity versus cycle number of various anode materials at the current density of 100 mA g^{-1}. Despite SiO nanoparticles electrode shows better cycling performance than as-received SiO electrode, a significant capacity fade occurs under 20 cycles. It is clear that much better cycling performance was obtained for the SiO/graphene electrode. The discharge capacity after 100 cycles for the SiO/graphene electrode is 890 mAh g^{-1}, much higher than that of the bare graphene electrode (383 mAh g^{-1}). Figure 3d shows the cyclic performance of SiO/graphene at various current densities. The cell was first cycled at 100 mA g^{-1} for 20 cycles, in which a stable reversible capacity of about 1049 mAh g^{-1} was observed. At the high current densities of 200, 400 and 800 mA g^{-1}, the SiO/graphene can still deliver high reversible specific capacity of 890, 701 and 441 mAh g^{-1}, respectively. When the current density returns to the initial 100 mA g^{-1} after more than 50 cycles, a stable high reversible specific capacity of 910 mAh g^{-1} can be recovered. We assume the high reversibility and rate capability of SiO/graphene nanocomposite is attributed mainly to the following points. The good mechanical flexibility of graphene can readily accommodate the large volume change associated with a conversion reaction electrode, and can prevent the aggregation of the SiO nanoparticles. The use of ultrafine SiO nanoparticles can also contribute to a reduction of the intrinsically large volume change during Li insertion/extraction process [28]. On the other hand, SiO nanoparticles on the surface of graphene can play a role in preventing the restacking of graphene with the loss of their active surface area [13,18]. In addition, graphene could also act as a three-dimensional conductive network for SiO nanoparticles, which could decreas the inner resistance of LIBs and promote the electrontransfer during the lithiation and delithiation process [27,29].

4. CONCLUSION

In summary, SiO/graphene nanocomposite was prepared successfully by an *in situ* chemical synthesis approach and investigated as the anode material in LIBs. FESEM, TEM and HRTEM

analysis shows the uniform dispersion of SiO nanoparticles (50-300 nm) on the planes of graphene. The SiO/graphene nanocomposite exhibits a large initial specific capacity of 2285 mAh g^{-1}, excellent cyclic performance of 890 mAh g^{-1} up to 100 cycles and good rate capability. It was found that the nanocomposite showed better cyclic performance than the pure SiO nanoparticles and bare graphene. The present results provide a new graphene-based composite anode material for energy storage applications in high-performance LIBs.

ACKNOWLEDGEMENTS
This work has been supported in part by National Natural Science Foundation of China (No. 50974045), the Ph. D Programs Foundation of Ministry of Education of China (No. 20092302110052) and the Natural Science Foundation of Heilongjiang Province, China (No. B200918).

References

1. G. Girishkumar, B. McCloskey, A. C. Luntz, S. Swanson, and W. Wilcke, *J. Phys. Chem. Lett.* 1 (2010) 2193.
2. Shi H, Barker J, Saidi MY, Koksbang R, *J. Electrochem. Soc.*143 (1996) 3466.
3. Jae-Hun Kim, Hun-Joon Sohn, Hansu Kim, Goojin Jeong, Wanuk Choi, *J. Power Sources*. 170 (2007) 456.
4. Angathevar Veluchamy, Chil-Hoon Doh, Dong-Hun Kim, *J. Power Sources*. 188 (2009) 574.
5. Q. Si, K.Hanai, T.Ichikawa, *J. Power Sources*. 196 (2011) 9774.
6. Xianxia Yuan, Ya-Jun Chao, Zi-Feng Ma, Xiaoyan Deng, *Electrochem. Commun.*. 9 (2007) 2591.
7. Jing Wang, Hailei Zhao, Jianchao He, Chunmei Wang, Jie Wang, *J. Power Sources*. 196 (2011) 4811.
8. A. Guerfi, P. Charest, M. Dontigny, *J. Power Sources*. 196 (2011) 5667.
9. Il Won Seong, Ki Tae Kim, Woo Young Yoon, *J. Power Sources*. 189 (2009) 511.
10. Il Won Seong, Woo Young Yoon, *J. Power Sources*. 195 (2010) 6143.
11. X.Li, Y.Zhu, W.Cai, M.Borysiak, B.Han, D.Chen, R.D.Piner, *Nano Lett.* 9 (2009) 4359.
12. Geim AK, *Science.* 324 (2009) 1530.
13. Zhifeng Du, Xiaoming Yin, Ming Zhang, *Materials Letters*. 64 (2010) 2076.
14. Gang Wang, Ting Liu, Yongjun Luo, *J. Alloys and Compounds*. 509 (2011) L216.
15. Gang Wang, Ting Liu, Xiaoling Xie, *Mater. Chem. Phys.* 128 (2011) 336.
16. Iresha R.M. Kottegoda, Nurul Hayati Idris, Lin Lu, *Electrochimica Acta.* 56 (2011) 5815.
17. Gang Wang, Jintao Bai, Yuhang Wang, *Scripta Materialia*. 65 (2011) 339.
18. Zhong-Shuai Wu, Wencai Ren, Lei Wen，*ACS Nano*. 4 (2010) 3187.
19. Y.J. Mai, X.L. Wang, J.Y. Xiang, Y.Q. Qiao, *Electrochimica Acta.* 56 (2011) 2306.
20. Z.S. Wu, W.C. Ren, L.B. Gao, B.L. Liu, C.B. Jiang, H.M. Cheng, *Carbon*. 47 (2009) 493.
21. Shuzhao Liang, Xuefeng Zhu, Peichao Lian, *J. Solid State Chem.*. 184 (2011) 1400.
22. Jae-Hun Kim, Cheol-Min Park, Hansu Kim, *J. Electroanal. Chem*. 661 (2011) 245.
23. Masayuki Yamada, Atsushi Ueda, Kazunobu Matsumoto and Tsutomu Ohzuku, *J. Electrochem. Soc*. 158 (2011) A417.
24. I. Francis Cheng, Yuqun Xie, *Carbon*. 49 (2011) 2852.
25. N. Wang, Y.H. Tang, Y.F. Zhang, *Chemical Physics Letters*. 299 (1999) 237.
26. Mariko Miyachi, Hironori Yamamoto, Hidemasa Kawai, *J. The Electrochem. Soc.*. 152 (2005) A2089.
27. Peng Guo, Huaihe Song, Xiaohong Chen, *Electrochem. Commun.*. 11 (2009) 1320.

28. L. Balan, J. Ghanbaja, P. Willmann, D. Billaud, *Carbon*. 43 (2005) 2311.
29. A. H. Castro Neto, F. Guinea, N. M. R. Peres, *Reviews of Modern Physics.* 81 (2009) 109.